SAE Technical Paper 2023-24-0059

# Comparison of Premixed Fuel and Premixed Charge Operation for Propane-Diesel Dual-Fuel Combustion

**Mueller F.[1], Guenthner M.[1]**
[1] RPTU University of Kaiserslautern-Landau

## Abstract

With the rising popularity of dual-fuel combustion, liquefied petroleum gas (LPG) can be utilized in high-compression diesel engines. Through production from biomass (biomass to liquid, BtL), biopropane as a direct substitute for LPG can contribute to a reduction in greenhouse gas emissions caused by combustion engines. In a conventional dual-fuel engine, the low reactivity fuel (LRF) propane is premixed with the intake air to form a homogeneous mixture. This air-fuel mixture is then ignited by the high reactivity fuel (HRF) in the form of a diesel pilot injection inside the cylinder. In the presented work, this premixed charge operation (PCO) is compared to a method where propane and diesel are blended directly upstream of the high-pressure pump (premixed fuel operation, PFO) in variable mixing ratios for different engine loads and speeds. Furthermore, the effects of internal and external exhaust gas recirculation are investigated for each operating mode. The results show that PCO allows higher propane ratios of up to 75 % at low loads, while PFO enables higher percentages of propane at medium and high loads (up to 50 %), allowing for a "reactivity on demand" approach. In addition, PFO shows significantly lower emissions of unburned hydrocarbons (-98.3 %) and carbon monoxide (-94.6 %) compared to PCO while soot emissions are reduced in both cases. The use of EGR allows nitrogen oxide emissions to be lowered to similar levels for both operation modes and shows benefits concerning unburned hydrocarbon (-73.5 %) and carbon monoxide (-62.9 %) emissions in PCO.

## 1. Introduction

The need to reduce greenhouse gas emissions has led to the development of different alternative powertrain technologies. While battery electric vehicles (BEV) are getting more and more popular for passenger cars [1], other areas of transportation, as well as working machines, have different requirements. These are not yet met by battery electric powertrains. As an alternative, conventional combustion engines can be de-fossilized using renewable fuels, which can either be produced from biomass or from green electric energy. In both cases, the carbon dioxide ($CO_2$) produced during combustion is part of a closed carbon cycle and therefore climate neutral. BioLPG, which consists mainly of propane, is an example for such a biofuel and is investigated in this work. The properties of BioLPG can be found in Table 3 (fuel properties for diesel are shown in Table 4). BioLPG is generated as a by-product of biodiesel production through hydrogenolysis (for 100 units of biodiesel 5 units of BioLPG are produced), produced by Neste Corporation in Rotterdam. In this process, the energy content of the raw materials is extracted and purified with the aid of hydrogen. About 60 % of the feedstocks for BioLPG are residual and waste materials, the other 40 % include vegetable oils derived from jatropha nuts, soybeans, rapeseed, palms and other plants [2].

As an additional measure to renewable fuels, engine efficiency must be increased. This can be achieved by the utilization of ultra-lean combustion. In a spark ignited engine, the limit of lean combustion under homogeneous conditions is determined by both the lean flammability limit of the fuel and the maximum energy the ignition system can deliver. Luszcz et al. [3] showed that traditional spark ignition without the use of a pre-chamber can enable stable combustion with gasoline until an air–fuel equivalence ratio of 1.9 is reached by utilizing 500 mJ high energy ignition coils. As an alternative to spark ignited operation for lean mixtures, dual-fuel (DF) combustion has gained popularity in recent years. In a dual-fuel engine, two fuels are used simultaneously in a compression ignition (CI) process. The so-called low-reactivity fuel (LRF) provides most of the energy and is ignited by a small portion of high-reactivity fuel (HRF) which delivers the ignition energy instead of a spark plug. By this process, LRFs which are normally not suitable for the use in CI applications can be burned at ultra-lean conditions. DF engines are typically based on diesel engines due to their high compression ratios, which are beneficial for engine efficiency. The option of diesel-only operation as a fallback solution is another advantage of this approach and allows for a higher fuel flexibility.

However, as diesel engines are not designed to run on homogeneous air-fuel mixtures – which is how the LRF is typically introduced into the combustion chamber – increased emissions of unburned hydrocarbons (THC) and carbon monoxide (CO) may become an issue, as underlined by numerous studies (e.g. [4–6]). This can be improved by the following measures:

- redesign of the combustion chamber / piston,
- internal and/or external exhaust gas recirculation (EGR),
- alternative DF combustion modes.

Nam et al. [7] showed the effect of different piston designs in a diesel-gasoline DF engine under a low load condition. Regarding CO and THC emissions, a mix between a conventional diesel and a gasoline bowl geometry showed the best results. Compared to a diesel piston, CO dropped from 19.32 g/kWh to 17.29 g/kWh and THC from 7.67 g/kWh to 7.04 g/kWh. The investigated bowl piston showed higher emissions of CO and THC with 24.85 g/kWh and 10.20 g/kWh respectively. On the downside, the mixed geometry showed a reduction in gross indicated efficiency of 1 % compared to the diesel piston. Splitter et al. [8] concluded that the biggest influence on these emission components comes from the squish volume with a need for

tight clearances between piston and cylinder wall. The best results were achieved with a bigger squish height between piston and cylinder head in combination with a larger bowl diameter. Belgiorno et al. [9] reduced the compression ratio of a methane-diesel DF engine while still keeping the omega-shaped piston bowl geometry. This led to a reduction in unburned methane ($CH_4$) emissions by up to 60 % but also decreased the BTE of the engine by about 3 %. This was mainly attributed to higher heat transfer losses with a reduced compression ratio.

The same authors also showed the potential of external EGR to reduce CO and THC emissions [9]. For an EGR rate of 35 %, these were decreased by 30 % and 37 %, respectively. The EGR also reduced the NOx emissions from 11 g/kWh down to 0.5 g/kWh. Because of the reduced diesel share, soot emissions did not increase with the EGR rate. Jost et al. [10] combined external EGR with internal EGR by exhaust gas rebreathing on a POMDME-methane DF engine. This was done by a second exhaust valve lift during the intake stroke and allowed for a reduction of $CH_4$ raw emissions by 63 %, while CO emissions were reduced by up to 80 %. Similar results were achieved through the same measures in a diesel-methane DF concept [11]. Dev et al. [12] investigated external EGR on a CNG-diesel DF engine. The results showed a slight reduction in $CH_4$ emissions when using EGR, while CO stayed at a similar level. NOx emissions were also reduced, and soot emissions only increased by a small fraction as a result of the reduced diesel share in DF mode. BTE dropped by up to 1 % at 50 % load when using EGR because of a decrease in combustion efficiency. At higher load, this was not observed and the BTE were identical with and without EGR. Zeraati-Rezaei et al. [13] showed the benefit of hot EGR when used with a 75 % gasoline, 25 % diesel mixture fueled premixed compression ignition (PCI) engine. Combined with low pressure injection, THC and CO emissions could be decreased as well as nitrogen oxide (NOx) and soot emissions while increasing combustion stability. PCI differs from conventional DF combustion through fuel premixing and early direct injection of this mixture.

The different combustion modes were summarized by Martin and Boehman in [14]. Based on Homogeneous Charge Compression Ignition (HCCI), where solely an LRF is used, and Premixed Charge Compression Ignition (PCCI) using only an HRF and early direct injection (DI), Reactivity-Controlled Compression Ignition (RCCI) as a combination of both has emerged as a promising combustion process. This concept combines an LRF – which is usually injected into the intake port – and an HRF introduced into the combustion chamber through early DI. The start of combustion is then determined by the ratio between LRF and HRF, as well as through the ambient conditions inside the cylinders such as charge temperature, pressure and EGR ratio. This enables a Low-Temperature Combustion (LTC) with very low raw emissions. Reitz and Duraisamy [15] investigated RCCI for different combinations of fuels, including a “single fuel strategy” approach by the use of an additive to influence reactivity. In every case, NOx and soot emissions were reduced by several orders of magnitude while the indicated engine efficiency was improved. The combination of E85 and diesel showed the highest thermal efficiency of 59 %. Similar observations were made by Benajes et al. [16]. Using diesel-gasoline RCCI, soot and NOx emissions could be improved, but THC and CO emissions increased. The reason was found to be crevices inside the combustion chamber where the LRF was harder to ignite and burn completely. Another possibility of using two fuels in the same engine is the separate direct injection of both fuels like demonstrated in [17]. Giramondi et al. used a diesel injection close to combustion TDC, followed by an injection of ethanol containing most of the released energy. The gross indicated efficiency revealed to be higher for this process than in diesel-only mode.

The Premixed Charge Operation (PCO) presented in this work matches with the classifications of Conventional Dual-Fuel (CDF) and Partial HCCI (PHCCI) according to the nomenclature introduced in [14]. When PHCCI combustion occurred, the homogeneously distributed fuel inside the cylinder was triggered to auto-ignite after the injection of the HRF but before the LRF was consumed by the flame front. This was caused by the increase in cylinder pressure caused by the combustion of the HRF in combination with high internal and external EGR rates. Kang et al. [18] investigated this type of combustion with diesel-propane DF using up to 65 % propane energy share, and demonstrated a reduction in soot emissions. While NOx stayed at a similar level, CO and THC emissions increased with the propane to diesel ratio. Yu et al. called this combustion process Homogeneous Charge Induced Ignition (HCII), [19]. In their investigation, they also found HCII capable of reducing both NOx and soot emissions, while enabling high thermal efficiencies. Using high EGR rates, they were capable to realize LTC with a further reduction in nitrogen oxides and soot emissions. In the same study, Gasoline/Diesel Blend Fuels (GDBF) combustion is investigated, which corresponds to the Premixed Fuel Operation (PFO) in this work. The thermal efficiency was similar or higher to conventional diesel CI combustion while soot emissions were reduced. While NO emissions were higher for the examined fuel blends (with a gasoline fraction between 0.2 and 0.8 of the total fuel energy), higher EGR rates were possible than with diesel only due to the mentioned reduction in soot, allowing to reduce NO to very low levels. The combustion mode fits the Conventional Diesel Combustion (CDC) definition according to [14]. Concerning blending propane and diesel, only few studies can be found. Qi et al. [20] investigated various blends of LPG and diesel, ranging from 0 % up to 40 % LPG, in a single cylinder engine. The results showed that ignition delay increased with the LPG-share and that engine efficiency suffered at low loads while staying at diesel-like levels at high loads. Concerning emissions, a reduction of NOx with the LPG share was observed with a simultaneous increase in THC. Cardone et al. [21] premixed a fixed mass ratio of 80 % diesel and 20 % propane and used an optical single cylinder engine to study the combustion processes. A variation of injection parameters was investigated and an optimized injection strategy was derived from the experiments. This allowed for a reduction in NOx and PM emissions, which could be attributed to lower flame temperatures through the visualization of the combustion.

In the work presented here, biopropane was investigated in a four-cylinder tractor diesel engine both in a conventional dual-fuel combustion and by blending it with diesel upstream of the high-pressure fuel pump, with the aim of further clarification of the potential of propane as a fuel in both operating modes. The propane share was variably controlled in both modes and the combustion, thermal efficiency and emissions were analyzed. Furthermore, the effect of internal EGR by exhaust gas rebreathing was studied for both operating modes and in combination with varying ratios of external EGR. As uncooled exhaust gas is reintroduced into the cylinder through rebreathing, it is possible to increase residual gas temperature and ratio in the cylinder beyond the level possible with conventional, cooled external EGR. This promises to improve CO and THC emissions even further. After a brief overview of the experimental setup and the methodology, both dual-fuel modes are compared in the results and discussion chapter.

## 2. Experimental Setup

All the tests were conducted on a modified John Deere 4045 four-cylinder diesel engine. The engine is equipped with a two-stage turbocharging system, with a (passive) wastegate only for the high-pressure stage. Consequently, the second turbocharger is always fed

with the entire exhaust gas flow. Table 1 shows the technical data of the base engine.

Table 1. Technical data of the JD4045 engine.

| | Value | Unit |
|---|---|---|
| Rated Power | 130 | kW |
| Rated Speed | 2100 | rpm |
| Peak Torque (@ 1600 rpm) | 703 | Nm |
| Displacement | 4.5 | $dm^3$ |
| Stroke | 127 | mm |
| Bore | 106.5 | mm |
| Compression Ratio | 17.3:1 | - |
| Valves per Cylinder | 4 | - |
| Emission Standard | EU Stage IV | - |

Since EU Stage V is the current emission standard for commercial vehicles, it is used as the reference for the tests. Table 2 shows the according limits for the individual exhaust gas components.

Table 2. EU Stage V emission limits for class NRE-v-6 [22].

| | Value | Unit |
|---|---|---|
| CO | 3.5 | g/kWh |
| THC | 0.19 | g/kWh |
| $NO_x$ | 0.4 | g/kWh |
| PM | 0.015 | g/kWh |
| PN | $1 \times 10^{12}$ | #/kWh |

To enable exhaust gas rebreathing, a new cylinder head has been designed, manufactured, and installed on the engine. This modification comprises the conversion of the engine from an overhead valve (OHV) design with only one camshaft to a double overhead camshaft (DOHC) layout. The cylinder head features a fully variable valve lift (VVL) system for the intake and the exhaust side. While the intake lift was kept at its maximum for the current investigations, the VVL on the exhaust side was used to vary the second exhaust valve lift (also called second event / SE) of the first exhaust valve of each cylinder between 0 (EV 1 min) and 1.9 mm (EV 1 max), as illustrated in Figure 1 in relation to firing TDC at 0 °CA. Due to the kinematics of the valvetrain, this variation also reduces the main lift during the exhaust stroke from 8.8 to 5 mm. The second exhaust valve always opens at full lift and without a second opening event. More details concerning the valvetrain can be found in [23] and [11].

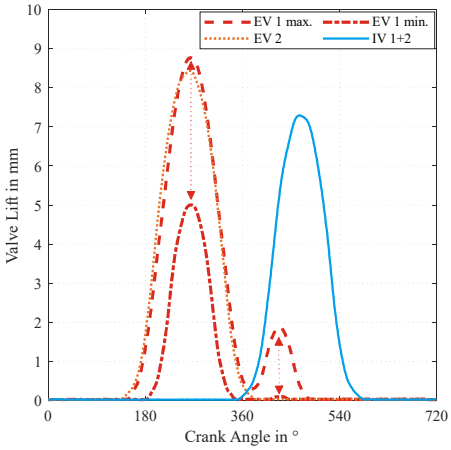


Figure 1: Measured valve lift characteristics (firing TDC = 0 °CA)

The propane was taken from the liquid phase of the tank, which was also put under additional pressure using nitrogen to avoid evaporation inside the fuel lines before injection. The properties of the used biopropane and diesel are displayed in Table 3 and Table 4.

Table 3. Properties of the used biopropane.

| | Testing standard | Value | Unit |
|---|---|---|---|
| Lower Heating Value (LHV) | Calculation based on propane and butane share | 46 | MJ/kg |
| Density (15 °C, Liquid Phase) | EN ISO 8973 | 510 | $kg/m^3$ |
| Motor Octane Number (MON) | DIN EN 289, Appendix B | 94.3 | - |
| Cetane Number | n.a., source: [20; 21] | < 3 | - |
| Propane Share | DIN EN 27941 | 76.66 | % (m/m) |
| Butane Share | Calculation based on propane share | 23.34 | % (m/m) |
| Carbon Content | Calculation based on propane and butane share | 82.53 | % (m/m) |
| Hydrogen Content | Calculation based on propane and butane share | 17.47 | % (m/m) |
| Stoichiometric Air–Fuel Ratio | Calculation based on carbon, hydrogen, oxygen and sulfur content [24] | 15.6 | - |
| Specific $CO_2$ Emission | Calculation based on carbon content and LHV | 65.78 | g/MJ |

Table 4. Properties of the used diesel EN590.

| | Testing standard | Value | Unit |
|---|---|---|---|
| Lower Heating Value (LHV) | DIN 51900-3:2005 | 42 | MJ/kg |
| Density (15 °C) | DIN EN ISO 12185:1997 | 833 | $kg/m^3$ |
| Cetane Number | EN 16715:2015 | 54 | - |
| Carbon Content | ASTM D5219-16 (Method C) | 86.20 | % (m/m) |
| Hydrogen Content | ASTM D5219-16 (Method C) | 13.40 | % (m/m) |
| Stoichiometric Air–Fuel Ratio | Calculation based on carbon, hydrogen, oxygen and sulfur content [24] | 14.5 | - |
| Specific $CO_2$ Emission | Calculation based on carbon content and LHV | 75.25 | g/MJ |

The PCO concept was enabled by installing a spacer between the intake manifold, which is integrated into the cylinder head, and the

EGR mixer. This spacer integrates four Bosch CNG injectors and also serves as a carrier for the corresponding fuel rail. The original direct injection fuel system was not modified for this operating mode. For PFO, a fuel mixer (Figure 2) was used to feed the original high-pressure fuel pump, rail and injectors. This mixer consists of eight low pressure fuel injectors (four for each fuel), which were installed on opposing sides of a mixing chamber and injected the respective amount of fuel for the desired mixing ratio. As this design requires a pressure drop between injector feed and mixing chamber, the pressure of diesel and propane was set to 13 bar. This allowed for a pressure of up to 12 bar at the intake of the high-pressure pump, which corresponds to a boiling temperature of 38 °C for pure propane.

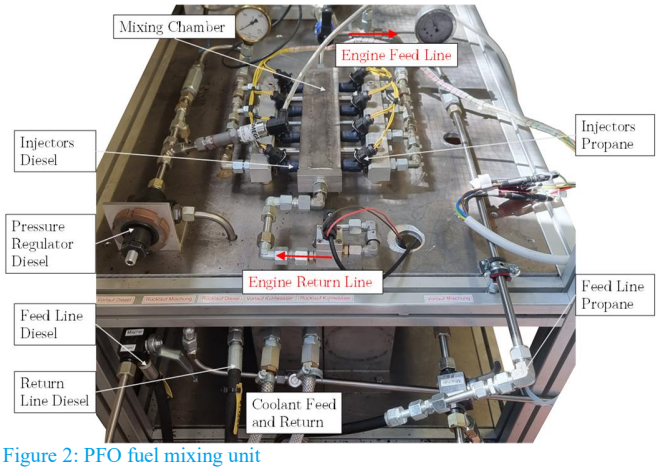

Figure 2: PFO fuel mixing unit

The load was applied by a Schenck W400 eddy current dyno. Every cylinder was fitted with a Kistler 6056 piezoelectric pressure sensor while Kistler 4011 piezoresistive low-pressure transducers were installed in the intake and exhaust manifold. A Heidenhain ROD 426 rotary encoder on the engine's crankshaft delivered the current crank angle with a resolution of 0.1 ° to the AVL Indimodul 621 and the corresponding IndiCom software for pressure indication and for detecting engine knock by analysis of the pressure signals during combustion. For static pressure measurements in the intake, exhaust, coolant and fuel system, a combination of Omega Engineering PXM 319 and Endress+Hauser Cerabar PMP21 were used. The exhaust gas temperatures were measured by Omega Engineering Type N thermocouples. For intake, coolant and fuel temperatures Omega Engineering PT100 probes were used. The airflow into the engine was determined by an ABB Sensyflow FMT700-P thermal mass flowmeter, while the mass flow of the diesel fuel was measured by an AVL FuelExact Coriolis flow meter, which also allowed for a conditioning of the diesel temperature to 20 °C. The propane mass flow was measured by a Endress+Hauser Cubemass C300 Coriolis mass flow meter. To determine the valve lifts, the eccentric shafts were fitted with Novotechnik RSC-2841 rotary sensors. For the exhaust gas measurements, a combination of a Horiba MEXA-6000FT Fourier-transform infrared spectrometer and a conventional Horiba MEXA-7000 exhaust gas analyzer was used for gaseous emissions, including the EGR rate, while an AVL Micro Soot sensor determined the concentration of particulate matter. The turbocharger speeds were measured by eddy current sensors from Micro Epsilon and the air-fuel ratio was determined by a Bosch LSU 5.1 wideband $O_2$ sensor in combination with an ETAS E635 lambda module. An overview of the measured and calculated values relevant for this study, including measurement accuracies and uncertainties, can be found in the appendix.

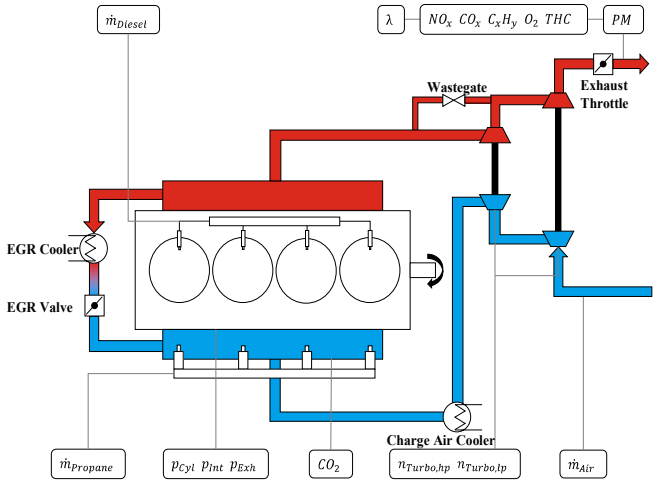

Figure 3: Test bench setup (schematic)

The original John Deere ECU was used to control injection timing, rail pressure, EGR valve and exhaust throttle position. For the propane injection, a MoTeC M800 ECU was used. In the PCO case it controlled the injectors in front of the intake manifold and enabled cylinder individual fuel trims to mitigate differences between the cylinders caused by the design of the manifold. For PFO, the eight injectors of the mixing chamber were defined as two pairs of four and were also controlled by the M800. The mixing ratio was set by shifting the balance between the two pairs.

## 3. Methodology

The experiments were conducted at four different load points. As a base operating point, a load of 350 Nm (equaling a BMEP of 9.8 bar) at 1600 min$^{-1}$ was chosen. This represents 50 % of the maximum engine torque at the engine speed for rated torque, which is relevant for the Non-Road Steady Cycle (NRSC) and the World Harmonized Stationary Cycle (WHSC). This is also the highest load at which the center of combustion can be kept at 8 °CA while the maximum cylinder pressure stays at or below the pressure limit of the engine (150 bar). The center of combustion $A_{i,50}$ represents the crank angle in relation to firing TDC at which 50 % of the thermal energy of the engine cycle has been released. It is calculated from the cumulative heat release $I(\alpha)$ by dividing it by its maximum value $I_{max}$ and then identifying the corresponding angle for $\frac{I(A_{i,50})}{I_{max}} = 0.5$.

From this intermediate load point, additional operating points were studied by reducing the torque to 175 Nm and increasing it to 525 Nm (4.9 and 14.7 bar BMEP, respectively) at the same engine speed to investigate the influence of engine load. Additionally, the engine speed was decreased to 1100 min$^{-1}$ at 350 Nm to cover the impact of varying engine speed at constant load. Although the BMEP and the engine speed were kept constant for each case respectively, the IMEP varied because of variations in efficiency losses caused by the investigated measures.

The exhaust throttle was always kept wide open, and the intake valves always opened to their full lift for every variation of propane substitution rate (SR), internal and external EGR. Through this approach, it was ensured that the engine always operated as lean as possible. Since the engine was not fitted with any active boost control to influence the wastegate position of the high-pressure turbocharger,

the EGR rate had a direct influence on the boost pressure and therefore on lambda.

The SR ($x_{Substitution}$) was defined as the ratio between the energy (as a product of fuel mass-flow $\dot{m}$ and lower heating value LHV) provided by the injected propane and the total energy supplied by diesel fuel and propane,

$$x_{Substitution} = \frac{\dot{m}_{Propane} * LHV_{Propane}}{\dot{m}_{Propane} * LHV_{Propane} + \dot{m}_{Diesel} * LHV_{Diesel}} * 100\ \%$$

According to the SR, the air–fuel equivalence ratio $\lambda$ was calculated using the fuel mass flows with their respective stoichiometric air demand and the air mass flow,

$$\lambda_{Mixture} = \frac{\dot{m}_{Air}}{\dot{m}_{Propane} * L_{st,Propane} + \dot{m}_{Diesel} * L_{st,Diesel}} * 100\ \%$$

The exhaust gas species concentrations $c_X$ were converted to brake specific emissions $bsX$ using the exhaust gas mass flow $\dot{m}_{Exh}$ (which consists of the air mass flow and the fuel mass flows), the brake engine power $P_e$, the molar mass of the components $M_X$ and the molar mass of the exhaust gas $M_{exh}$ (28.9 g/mol) according to the Stage V regulation [22],

$$bsX = \frac{c_X}{\dot{m}_{Exh} * P_e} * \frac{M_X}{M_{Exh}}$$

The ignition delay was defined as the crank angle between start of injection and 5 % mass burned fraction. The interval between 5 % and 90 % mass burned fraction was evaluated as the burn duration.

For every SR, the external EGR rate was then varied from 0 % up to 25 % (if possible) with an increment of 5 %. The second event valve lifts of 0, 0.5, 1.0, 1.5 and 1.9 mm were measured for each combination of SR and external EGR rate.

For every measurement, the center of combustion was kept constant at 8 °CA ATDC, with exception for the high-load point of 525 Nm. At this point, the start of combustion was retarded just as much as necessary to stay within the cylinder pressure limit. The diesel rail pressure was set to 1700 bar, or respectively 1470 bar for the 175 Nm low-load point.

## 4. Results and Discussion

As the low-load point of 175 Nm / 4.9 bar BMEP showed the least engine knock, a SR of 75 % was possible for PCO mode. In PFO, a reduction in rail pressure from 1470 bar to 1000 bar was necessary above 35 % SR. The fuel gets hotter the more it is pressurized in the high-pressure fuel pump through the mechanical work performed on it. As it returns to a lower pressure inside the fuel return system, it remains at the same temperature which makes this the critical point where evaporation occurs. Therefore, a reduction of rail pressure also reduces the fuel return temperature inside the low-pressure mixing circuit and prevents the propane from evaporating inside the fuel system. The mixing of propane with diesel leads to an elevation of the boiling-point for propane, meaning that its boiling point depends on the diesel share and therefore on the SR. With an increase in SR, the boiling point is therefore reduced, and the fuel return temperature becomes a critical value. Consequently, a fuel return temperature below the boiling point of pure propane (38 °C at 12 bar) would be the optimum but cannot be reached because of the heat transfer from the engine, which houses a part of the fuel return system. By decreasing the rail pressure, a SR of 50 % was achieved. A higher propane share would have been possible with a further reduction in rail pressure but was not investigated to avoid damage to the high-pressure fuel pump due to reduced lubrication by the fuel mixture. Figure 4 shows the trade-off between nitrogen oxides and soot for both operating modes. The transition from a diffusion flame to a lean flame front combustion for PCO showed a reduction in nitrogen oxides due to decreased peak temperatures inside the cylinders. For PFO, NOx stayed at the same level for every SR except for 50 %, where the deviation was caused by the decrease in injection pressure. For soot emissions, both modes showed a reduction with the increase in propane share. However, this decrease was mitigated for PFO when the rail pressure had to be reduced, resulting in similar soot levels to 35 % SR at 1470 bar.

With the decreasing diesel portion in PCO, the NOx-soot trade-off was no longer present. This occurred below a diesel injection mass of 20 mg per stroke, below which locally rich regions were avoided and therefore prevented the formation of soot. For PFO, the trade-off was always visible, as the mass of fuel injected directly into the combustion chamber was only slightly reduced.

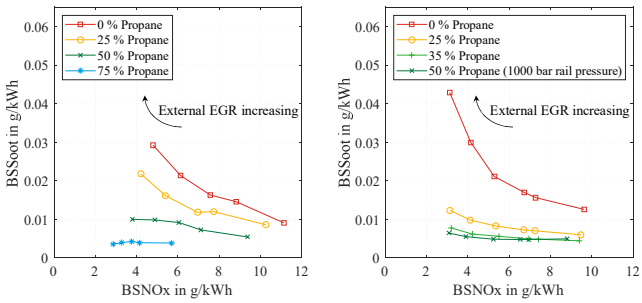


Figure 4: NOx-soot trade-off for PCO (left) and PFO (right) for different SR at 0 mm second event, external EGR in steps of 5 % starting at 0 % (1600 min$^{-1}$, 175 Nm)

Concerning CO and THC emissions, PCO showed a steep increase, while in PFO both components constantly remained just marginally above 0 g/kWh, with a minor increase corresponding to the reduced injection pressure at 50 % propane share, cf. Figure 5. The reason for the increase in PCO mode was the flame front type of combustion of the lean homogenous air-fuel mixture inside the combustion chamber. This flame front propagates rather slowly, which leads to it being extinguished during the expansion stroke. The reason for this is the high heat capacity of the cylinder charge caused by the lean mixture. This in turn resulted in unburned components at the end of combustion. Since these emissions are a result of incomplete oxidation and therefore need to be compensated by additionally injected fuel to maintain the heat release necessary for the operating point, both indicated and brake thermal efficiency (BTE) declined with the SR for PCO. The difference between these two efficiency values (ΔTE) – as a measure for engine friction – also declined with increasing SR. The reason for this could be found in the reduction in diesel fuel flow, which in turn reduced the power requirement for the high-pressure fuel pump. In PFO, brake thermal efficiency remained constant with an increasing difference between brake and indicated efficiency (ITE). With the increasing propane share, the volumetric energy density of the mixture is reduced, leading to a higher volumetric fuel consumption of the engine and therefore higher power consumption of the high-pressure fuel pump. This was also noticeable as the rail pressure reduction at 50 % SR led to a drop in friction losses.

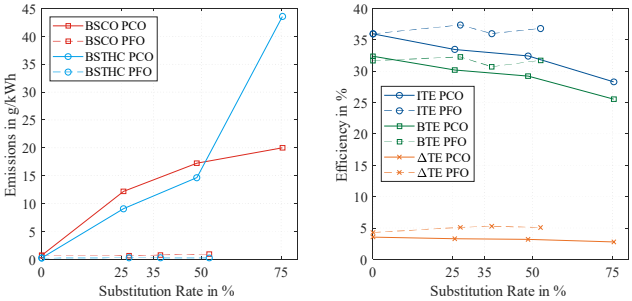


Figure 5: CO, THC (left), indicated, brake and delta efficiency (right) for PCO and PFO depending on SR at 0 mm second event, 0 % external EGR (1600 min$^{-1}$, 175 Nm)

To reduce these emissions, an elevation of the charge temperature was investigated. This was realized by the addition of internal and external EGR and a combination of both. Figure 6 shows the results for a SR of 75 % in PCO mode. To compare the influence of both EGR sources, the emissions are shown as a function of lambda. When compared to the base results without any second event (thus no internal EGR) and without external EGR, a combination of 1.9 mm second event valve lift and 20 % external EGR reduced the CO emissions by 62.9 % and THC by 73.5 %. Even though these measures led to higher charge temperatures, the nitrogen oxides were reduced by the lower concentration of oxygen inside the combustion chamber, resulting in slower combustion and lower peak temperatures. The prolonged combustion helps to keep in-cylinder temperatures at a higher level for a longer time during expansion, and thus above the oxidation temperature of THC (mainly propane $C_3H_8$) and CO. The evidence for this was already shown in [11] for diesel-methane DF combustion in PCO mode.

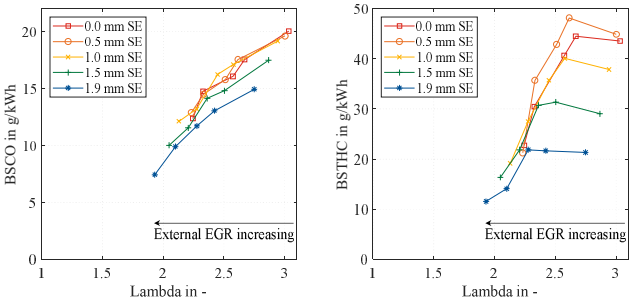


Figure 6: CO (left) and THC (right) for PCO depending on external and internal EGR at 75 % SR, external EGR in steps of 5 % starting at 0 % (1600 min$^{-1}$, 175 Nm)

In PFO mode, CO and THC emissions started at a lower level due to the diffusion flame type of combustion. As there is no homogeneously premixed fuel inside the cylinder at the start of the direct injection, there is also no flame front propagating through the combustion chamber. The second event operation therefore also provided less improvement compared to PCO (Figure 7), whereas external EGR did not affect the emissions of THC at all and led to an increase in CO emissions when approaching stoichiometric operation.

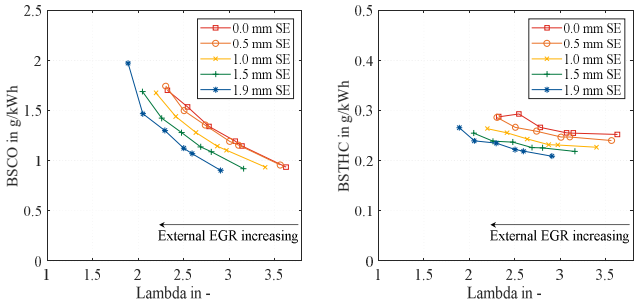


Figure 7: CO (left) and THC (right) for PFO depending on external and internal EGR at 50 % SR (1600 min$^{-1}$, 175 Nm)

As there was a lower potential for a further reduction of unburned components in PFO, the thermal efficiency of the engine was not as strongly influenced by these measures as in PCO. As obvious from Figure 8, the indicated and brake efficiency increased slightly with higher second event valve lift and external EGR due to reduced engine throttling. In PCO mode, efficiency depended more significantly on both internal and external EGR due to the additional effect of enabling a more complete combustion through these measures.

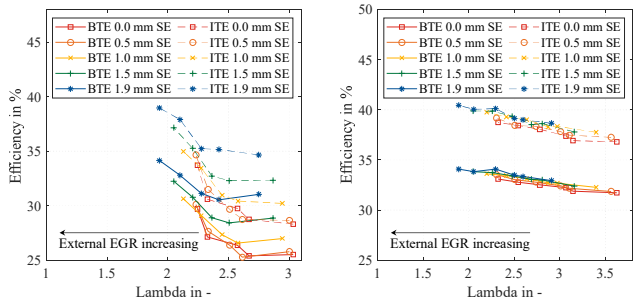


Figure 8: Indicated and brake efficiency for PCO (left, 75 % SR) and PFO (right, 50 % SR) depending on external and internal EGR, external EGR in steps of 5 % starting at 0 % (1600 min$^{-1}$, 175 Nm)

The reduced throttling is illustrated in Figure 9. As pumping work is reduced through the second event and/or external EGR, less energy needs to be released in the high-pressure loop for the same brake power, thus improving process efficiency. For the second event, there are two main effects which are responsible for the reduction of pumping work: firstly, the aforementioned higher main exhaust valve lift and opening duration for EV 1 on each cylinder during the exhaust stroke (increasing with the second event valve lift) and secondly the simultaneous opening of three valves during the intake stroke.

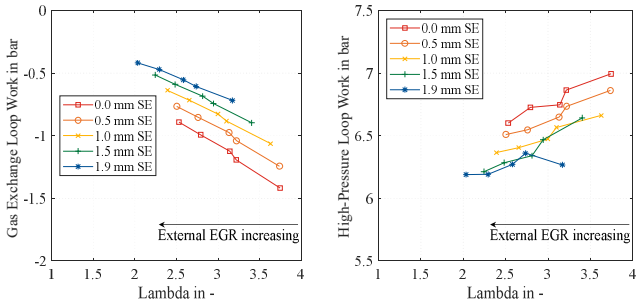


Figure 9: Gas exchange (left) and high-pressure loop work (right) for both modes depending on external and internal EGR, 0 % SR, external EGR in steps of 5 % starting at 0 % (1600 min$^{-1}$, 175 Nm)

Figure 10 and Figure 11 show the transition from a diffusion flame to a flame front in PCO as the heat release changes to a much flatter curve with a less distinctive peak. This is also the reason for the lower

nitrogen oxide emissions for increasing SRs, as the energy is released over a longer period of time with a reduced heat release rate, leading in turn to lower peak temperatures. However, at a SR of 75 % with 1.9 mm second event lift and 20 % external EGR, the heat release rate showed a second peak as the propane started to homogeneously auto-ignite after the diffusion combustion of the remaining diesel share (first peak), which corresponds to the PHCCI combustion process.

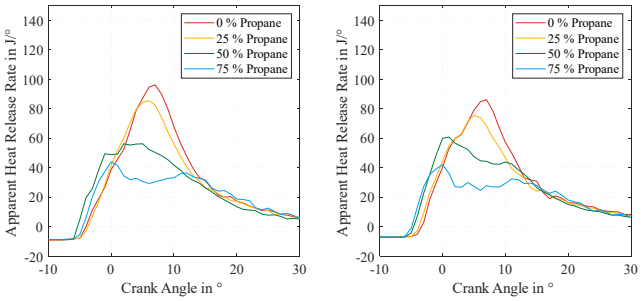


Figure 10: Heat release rate for 0 mm second event, 0 % external EGR (left) and 0 mm second event, 20 % external EGR (right) for PCO (1600 min$^{-1}$, 175 Nm)

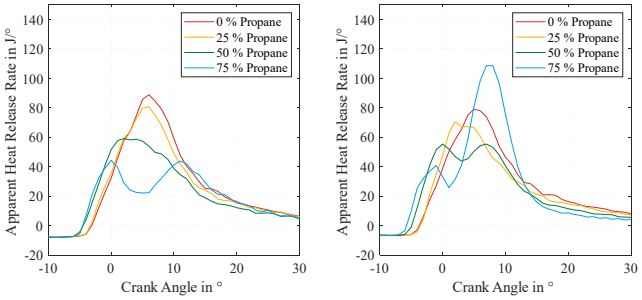


Figure 11: Heat release rate for 1.9 mm second event, 0 % external EGR (left) and 1.9 mm second event, 20 % external EGR (right) for PCO (1600 min$^{-1}$, 175 Nm)

This is also visible in both ignition delay and burn duration in Figure 12. The measurement points for the same second events lift are connected by lines for each SR. As the situation at a SR of 75 % was close to auto-ignition conditions for propane, the ignition delay and burn duration varied strongly. For the other SRs, a slight increase in burn duration with rising propane share could be observed without EGR. As soon as EGR was added, the burn duration of all variants converged to a rather narrow range. As the ignition delay only depends on the ignition of the diesel share, no significant differences could be detected in this variation.

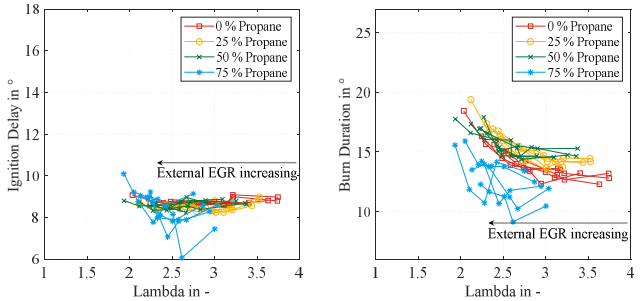


Figure 12: Ignition delay (left) and burn duration (right) for all second event lifts and external EGR rates in PCO, external EGR in steps of 5 % starting at 0 % (1600 min$^{-1}$, 175 Nm)

In the case of PFO, the differences in the heat release rate were smaller. As obvious from Figure 13, the gradient of the curve became steeper for increasing SRs, with an exception for the 50 % case with reduced injection pressure. While diesel-only combustion showed the tallest and most slim peak for no internal nor external EGR (Figure 13, left), this turned into the opposite as soon as EGR was added (Figure 13, right).

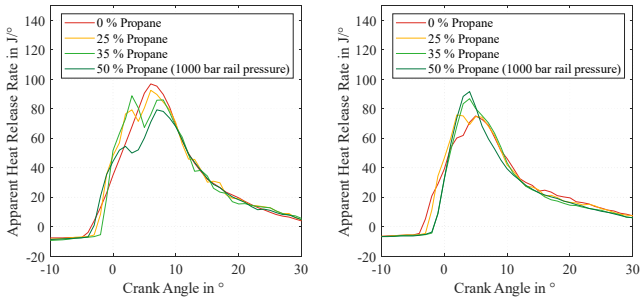


Figure 13: Heat release rate for 0 mm second event, 0 % external EGR (left) and 1.9 mm second event, 20 % external EGR (right) for PFO (1600 min$^{-1}$, 175 Nm)

Regarding the ignition delay, PFO showed a slight reduction for 25 % SR, while 50 % substitution led to a significant increase due to the reduction in rail pressure and the resulting deterioration of mixture formation. Burn duration decreased with the increase in propane share, again with the exception of 50 % SR (for the same reason). From its trajectory, this case also differed regarding the influence of external EGR. The burn duration showed a small influence of the second event lift, but the typical increase with rising EGR rates disappeared. This was caused by the higher ignition delay at this SR. At this engine speed and load, the injection duration was 1.15 ms, whereas the ignition delay of 12 °CA corresponds to 1.25 ms. This means that injection was already completed before the start of combustion occurred.

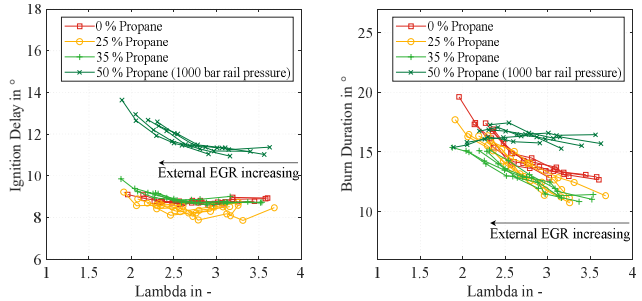


Figure 14: Ignition delay (left) and burn duration (right) for all second event lifts and external EGR rates in PFO, external EGR in steps of 5 % starting at 0 % (1600 min$^{-1}$, 175 Nm)

At an increased load of 350 Nm and the same engine speed of 1600 min$^{-1}$, PCO was limited to a SR of 30 % due to the occurrence of knock. For PFO, there was no influence on the SR, which could be maintained at 50 % for the reduced rail pressure of 1000 bar. Figure 15 illustrates that the reduction in rail pressure led to a higher soot level at 50 % SR than observed with 1700 bar injection pressure at 25 % propane share. Consequently, a further reduction in rail pressure was not investigated.

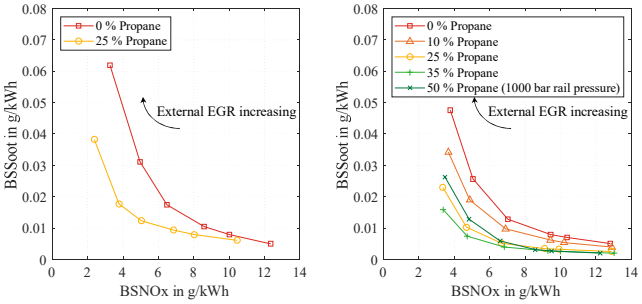


Figure 15: NOx-soot trade-off for PCO (left) and PFO (right) for different SR at 0 mm second event, external EGR in steps of 5 % starting at 0 % (1600 min$^{-1}$, 350 Nm)

Due to the higher heat release at increased load, the emissions of CO and THC did not increase as much as at the lower load point for PCO. At a SR of 25 %, CO dropped from 12.2 g/kWh to 6.5 g/kWh and THC from 9.1 g/kWh to 1.9 g/kWh without the use of a second event or external EGR, cf. Figure 16. As a result, the engine efficiency also remained on a similar level as without propane substitution. PFO showed diesel-like emissions and efficiency over the entire range of substitution shares.

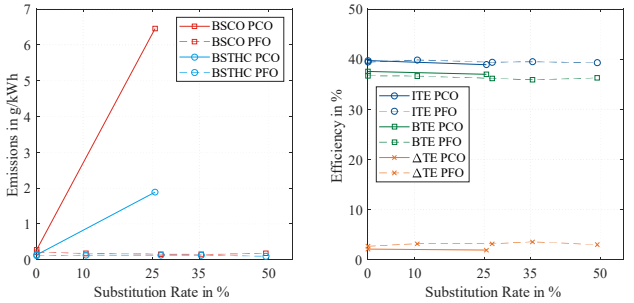


Figure 16: CO, THC (left), indicated, brake and delta efficiency (right) for PCO and PFO depending on SR at 0 mm second event, 0 % external EGR (1600 min$^{-1}$, 350 Nm)

At 1100 min$^{-1}$ and 350 Nm, PCO and PFO were comparable in terms of maximum SR at 45 % and 40 %, respectively. The higher knock limit for PCO was caused by the lower cylinder pressure when compared to the same load at 1600 min$^{-1}$. In PFO, the rail pressure had to be reduced to 1500 bar for 30 % SR and to 1200 bar for 40 % due to the engine's high fuel return flow at this speed. Since this operating point was rather rich – due to the insufficient fit of the turbochargers for this operation – and therefore restricted by high soot formation, the possible external EGR rates were also constrained, especially for high second event valve lifts. On the other hand, the knock limitation could be mitigated by a reduction in cylinder pressure through dethrottling of the engine using second event and external EGR. As a compromise, the EGR and SR variation are shown for a second event lift of 1.5 mm for both operating modes in Figure 17. The curves for 0 % propane differed slightly between PCO and PFO due to varying ambient conditions at the test bench and a lack of intake air conditioning, but overlapped on the same trajectory. PCO had a bigger impact on both NOx and soot emissions, while an increase in propane share over 10 % showed no benefit in soot for PFO due to the lower injection pressures.

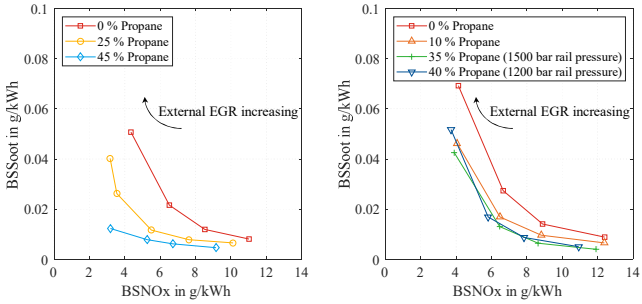


Figure 17: NOx-soot trade-off for PCO (left) and PFO (right) for different SR at 1.5 mm second event, external EGR in steps of 5 % starting at 0 % (1100 min$^{-1}$, 350 Nm)

As the absolute time for oxidation was prolonged by the reduced engine speed, the emissions of THC and CO were lower in PCO than at the 1600 min$^{-1}$, 350 Nm operating point. As before, PFO did not show a relevant increase in these emissions with the SR. This also means that the indicated efficiency stayed at an almost constant level for all SR. Friction increased with SR for PFO, while it decreased for PCO, making PCO more efficient in terms of brake thermal efficiency at high propane shares, Figure 18.

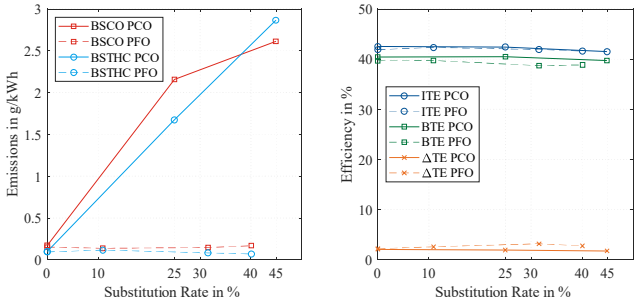


Figure 18: CO, THC (left), indicated, brake and delta efficiency (right) for PCO and PFO depending on SR at 1.5 mm second event, 0 % external EGR (1100 min$^{-1}$, 350 Nm)

The correlation between engine speed or engine load and the unburned emission components is shown for the same SR in Figure 19. With a reduction in BMEP at constant engine speed, the in-cylinder pressure and temperature decreased, promoting an increase of THC and CO. When BMEP was kept constant and engine speed was reduced, the absolute process time at elevated temperatures was prolonged, which proved beneficial for the oxidation of CO and THC. This behavior could also be observed for diesel-only combustion (0 % propane in Figure 19), but at a much lower level than in PCO mode.

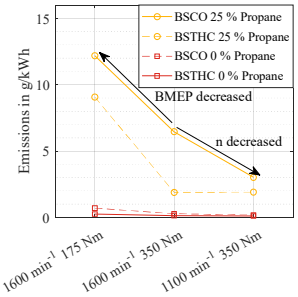


Figure 19: Influence of engine speed and load on CO and THC for PCO at 0 mm second event and 0 % external EGR

A further increase in engine load to 525 Nm at 1600 min$^{-1}$ led to excessive engine knocking in PCO mode. This limited the SR to 15 % in order to avoid damage to the engine, with no possibility of utilizing

external EGR. As a result, no statement can be made regarding the NOx-soot trade-off for this mode. PFO was not affected by this problem and was operated with a maximum SR of 40 %. As the rail pressure had to be reduced to 1400 bar, the reduction in soot formation compared to 25% propane share was rather small.

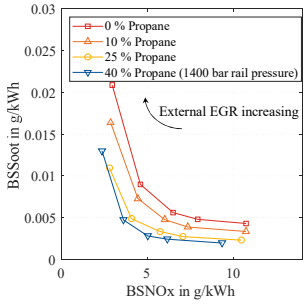


Figure 20: NOx-soot trade-off for PFO for different SR at 0 mm second event, external EGR in steps of 5 % starting at 0 % (1600 min$^{-1}$, 525 Nm)

Regarding engine efficiency as well as CO and THC emissions, the behavior in both PCO and PFO mode was similar to the load points at 350 Nm, see Figure 21. Again, as the injection pressure needed to be reduced for 40 % SR in PFO mode, CO emissions increased slightly.

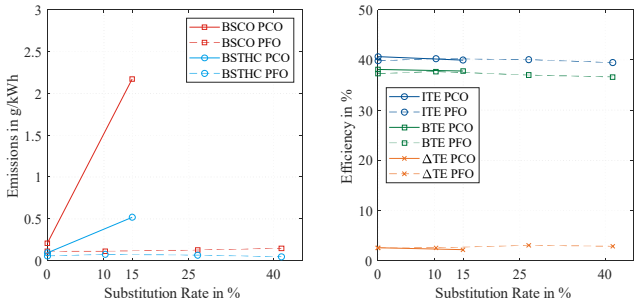


Figure 21: CO, THC (left), indicated, brake and delta efficiency (right) for PCO and PFO depending on SR at 0 mm second event, 0 % external EGR (1600 min$^{-1}$, 525 Nm)

The lack of external EGR in PCO means that the emissions of CO and THC could only be decreased through the application of a second event valve lift. Concerning CO, an adjustment from 0 mm to 1.9 mm led to a decrease from 2.2 g/kWh to 1.8 g/kWh, while THC remained almost constant.

Figure 22 shows the summarized limits of the SR for each mode under the boundary conditions set for these investigations which can be found in the methodology section.

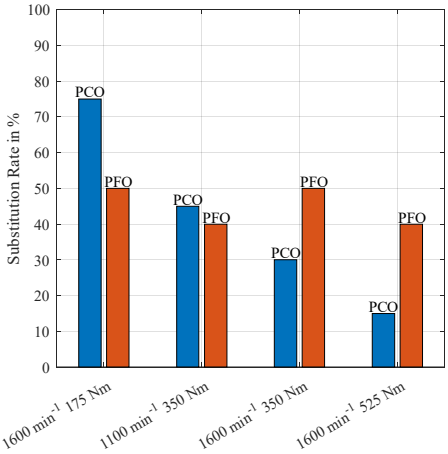


Figure 22: Substitution rate depending on operating point

## 5. Summary and Conclusion

In the presented work, two different dual-fuel operating modes were investigated. The premixed charge operation (PCO) corresponds to a conventional dual-fuel combustion where the low reactivity fuel (LRF) biopropane is introduced into the intake manifold and ignited by the high reactivity fuel (HRF) diesel inside the cylinder. In premixed fuel operation (PFO), both fuels were premixed directly upstream of the high-pressure pump and burned through a conventional diesel combustion (CDC). To reduce emissions, internal EGR by exhaust gas rebreathing enabled by a second exhaust valve lift during the intake stroke was investigated, as well as an external, cooled high-pressure EGR. The following observations have been made:

- PCO led to a decrease in nitrogen oxides (NOx) and soot emissions and to an increase in carbon monoxide (CO) and unburned hydrocarbons (THC) emissions, compared to diesel-only combustion. The combination of internal EGR – by exhaust gas rebreathing – and external EGR proved to be an effective measure to reduce both CO and THC emissions by up to 62.9 % and 73.5 %, respectively. This measure also helped to improve the BTE, which was reduced with the propane share at the low load point if no EGR was used. The SR was limited due to engine knock depending on the engine load point and speed.

- PFO mode showed no increases of CO and THC emissions compared to diesel-only combustion. NOx emissions stayed at a similar level, the BTE dropped slightly because of increased friction in the high-pressure fuel pump. Soot formation was reduced with an increase in propane share. PFO did not show any limitations due to knock, but with an increase in substitution rate, the fuel temperature of the engine return line became an issue. This was especially relevant at the lower engine speed of 1100 min$^{-1}$. Since a further increase in the fuel pressure of the mixture loop was not possible, a decrease in rail pressure, which in turn reduced the fuel return temperature, was a measure to avoid the evaporation of the propane share at this point. The rail pressure was reduced only until the benefit in the NOx-soot trade-off was mitigated, which in turn was a boundary condition during the investigation. With a further reduction of the rail pressure, higher substitution rates would have been possible. This would also reduce the nitrogen oxide emissions but might further mitigate the benefits of the reduction in soot formation by propane addition. As the efficiency losses increased with the substitution rate because of the higher parasitic work of the high-pressure pump, this reduction

in rail pressure helped to reduce the efficiency loss. However, any increase of the propane share leads to a decrease of fossil carbon dioxide emissions as the propane used for the study was derived from renewable sources.

For further investigations, a combination of PCO and PFO appears promising to maximize the substitution of diesel by propane. As PCO allowed a substitution rate of 75 % at 1600 $min^{-1}$ and 175 Nm, 25 % of diesel share remained at this point. If the results of 50 % substitution for PFO at this point are applied to the diesel share, the overall substitution rate could, in theory, be raised to 87.5 % or even higher. As the flame front combustion in PCO mode also decreased soot emissions, EGR could possibly be increased even further. This also means that a reduction in rail pressure would not affect the soot formation as much as in PFO-only mode, which in turn might enable higher SR through a further decrease in rail pressure. The same logic applies to the remaining load points. To decrease engine knock in PCO mode, the fully variable valvetrain on the intake side could be modified to enable early or late intake valve closing (IVC) to decrease the effective compression ratio in higher load points.

## Contact Information

Dipl.-Ing. Florian Mueller

RPTU University of Kaiserslautern-Landau, Germany
Institute of Vehicle Propulsion Systems (LAF)
D-67663 Kaiserslautern/Germany

E-Mail: florian.mueller@mv.rptu.de

## Acknowledgements

The work presented here was carried out as part of the project “High-Efficiency Dual-Fuel Combustion” (HKMVK), funded by the German Federal Ministry of Food and Agriculture (BMEL) with the Agency for Renewable Resources (FNR) as project management organization. The authors would like to express their gratitude for this funding.
Furthermore, the authors would like to thank the associated project partner John Deere for their support throughout the project.

# References

[1] Kraftfahrtbundesamt, “Pressemitteilungen - Der Fahrzeugbestand am 1. Januar 2023.” [Press releases - The vehicle fleet on January 1, 2023] 2023. Accessed March 20, 2023. https://www.kba.de/DE/Presse/Pressemitteilungen/Fahrzeugbestand/2023/pm08_fz_bestand_pm_komplett.html

[2] Primagas, “Bio-Flüssiggas: Herstellung, Anwendung und mehr.” [Bio-LPG: Production, application and more] 2023. Accessed March 20, 2023. https://fluessiggas.de/wissen/fluessiggas/biolpg/

[3] Luszcz, P., Takeuchi, K., Pfeilmaier, P., Gerhardt, M., Adomeit, P., Brunn, A., Kupiek, C., and Franzke, B., “Homogeneous lean burn engine combustion system development – Concept study." 2018, *In: Bargende, M., Reuss, H.-C., and Wiedemann, J. (eds), 18th International Stuttgart Symposium, Proceedings*. Springer Vieweg, Wiesbaden, pp. 205–223, https://doi.org/10.1007/978-3-658-21194-3_19

[4] Benajes, J., Garcia, A., Monsalve-Serrano, J., and Boronat, V., “Dual-Fuel Combustion for Future Clean and Efficient Compression Ignition Engines.” 2017. *Applied Sciences,* https://doi.org/10.3390/app7010036

[5] Chaichan, M. T., “Combustion of Dual Fuel Type Natural Gas/Liquid Diesel Fuel in Compression Ignition Engine.” 2014. *IOSR Journal of Mechanical and Civil Engineering*, no. 6: pp. 48–58, https://doi.org/10.9790/1684-11644858

[6] Jha, P. R., Partridge, K. R., Krishnan, S. R., and Srinivasan, K. K., “Impact of low reactivity fuel type on low load combustion, emissions, and cyclic variations of diesel-ignited dual fuel combustion.” 2023. *International Journal of Engine Research* 24 (1): pp. 42–63, https://doi.org/10.1177/14680874211041993

[7] Nam, T., Chu, S., Moon, S., and Min, K., “Effects of Piston Bowl Geometries on Diesel and Gasoline Dual-Fuel Combustion under Low Load Conditions.” 2022. *Int.J Automot. Technol.* 23 (4): pp. 993–1002, https://doi.org/10.1007/s12239-022-0086-y

[8] Splitter, D., Wissink, M., Kokjohn, S., and Reitz, R. D., “Effect of Compression Ratio and Piston Geometry on RCCI Load Limits and Efficiency." 2012, *SAE Technical Paper Series*. SAE International400 Commonwealth Drive, Warrendale, PA, United States, SAE Technical Paper 2012-01-0383, https://doi.org/10.4271/2012-01-0383

[9] Belgiorno, G., Di Blasio, G., and Beatrice, C., “Parametric study and optimization of the main engine calibration parameters and compression ratio of a methane-diesel dual fuel engine.” 2018. *Fuel* 222: pp. 821–840, https://doi.org/10.1016/j.fuel.2018.02.038

[10] Jost, A.-K., Günthner, M., Müller, F., and Weigel, A., “Investigation of an Engine Concept for CNG-OME Dual Fuel Operation Using External and Internal EGR." 2022, *SAE Technical Paper Series*. SAE International400 Commonwealth Drive, Warrendale, PA, United States, SAE Technical Paper 2022-32-0067, https://doi.org/10.4271/2022-32-0067

[11] Mueller, F., Guenthner, M., Weigel, A., and Thees, M., “Investigation of a Second Exhaust Valve Lift to Improve Combustion in a Methane - Diesel Dual-Fuel Engine." 2022, *SAE Technical Paper Series*. SAE International400 Commonwealth Drive, Warrendale, PA, United States, SAE Technical Paper 2022-01-0466, https://doi.org/10.4271/2022-01-0466

[12] Dev, S., Guo, H., Lafrance, S., and Liko, B., “An Experimental Study on the Effect of Exhaust Gas Recirculation on a Natural Gas-Diesel Dual-Fuel Engine." 2020, *SAE Technical Paper Series*. SAE International400 Commonwealth Drive, Warrendale, PA, United States, SAE Technical Paper 2020-01-0310, https://doi.org/10.4271/2020-01-0310

[13] Zeraati-Rezaei, S., Al-Qahtani, Y., and Xu, H., “Investigation of hot-EGR and low pressure injection strategy for a Dieseline fuelled PCI engine.” 2017. *Fuel* 207: pp. 165–178, https://doi.org/10.1016/j.fuel.2017.05.078

[14] Martin, J., and Boehman, A., “Mapping the combustion modes of a dual-fuel compression ignition engine.” 2022. *International Journal of Engine Research* 23 (9): pp. 1453–1474, https://doi.org/10.1177/14680874211018376

[15] Reitz, R. D., and Duraisamy, G., “Review of high efficiency and clean reactivity controlled compression ignition (RCCI) combustion in internal combustion engines.” 2015. *Progress in Energy and Combustion Science* 46: pp. 12–71, https://doi.org/10.1016/j.pecs.2014.05.003

[16] Benajes, J., Molina, S., García, A., Belarte, E., and Vanvolsem, M., “An investigation on RCCI combustion in a heavy duty diesel

engine using in-cylinder blending of diesel and gasoline fuels." 2014. *Applied Thermal Engineering* 63 (1): pp. 66–76, https://doi.org/10.1016/j.applthermaleng.2013.10.052

[17] Giramondi, N., Jäger, A., Norling, D., and Erlandsson, A. C., "Influence of the diesel pilot injector configuration on ethanol combustion and performance of a heavy-duty direct injection engine." 2021. *International Journal of Engine Research* 22 (12): pp. 3447–3459, https://doi.org/10.1177/14680874211001260

[18] Kang, J., Chu, S., Lee, J., Kim, G., and Min, K., "Effect of operating parameters on diesel/propane dual fuel premixed compression ignition in a diesel engine." 2018. *Int.J Automot. Technol.* 19 (1): pp. 27–35, https://doi.org/10.1007/s12239-018-0003-6

[19] Yu, C., Wang, J., Wang, Z., and Shuai, S., "Comparative study on Gasoline Homogeneous Charge Induced Ignition (HCII) by diesel and Gasoline/Diesel Blend Fuels (GDBF) combustion." 2013. *Fuel* 106: pp. 470–477, https://doi.org/10.1016/j.fuel.2012.10.068

[20] Qi, D. H., Bian, Y., Ma, Z., Zhang, C., and Liu, S., "Combustion and exhaust emission characteristics of a compression ignition engine using liquefied petroleum gas–Diesel blended fuel." 2007. *Energy Conversion and Management* 48 (2): pp. 500–509, https://doi.org/10.1016/j.enconman.2006.06.013

[21] Cardone, M., Mancaruso, E., Marialto, R., Sequino, L., and Vaglieco, B. M., "Characterization of Combustion and Emissions of a Propane-Diesel Blend in a Research Diesel Engine." 2016, *SAE Technical Paper Series*. SAE International400 Commonwealth Drive, Warrendale, PA, United States, 2016-01-0810, https://doi.org/10.4271/2016-01-0810

[22] European Parliament and Council, "Regulation (EU) 2016/1628 of the European Parliament and of the Council." 2016. https://eur-lex.europa.eu/eli/reg/2016/1628/oj

[23] Buitkamp, T., Günthner, M., Müller, F., and Beutler, T., "A detailed study of a cylinder activation concept by efficiency loss analysis and 1D simulation." 2020. *Automot. Engine Technol.* 5 (3-4): pp. 159–172, https://doi.org/10.1007/s41104-020-00070-1

[24] Mollenhauer, K., "Motortechnische Grundlagen des Dieselmotors." 2018, *In: Tschöke, H., Mollenhauer, K., and Maier, R. (eds), Handbook of Diesel Engines*. Springer Vieweg, Wiesbaden, pp. 13–26, https://doi.org/10.1007/978-3-658-07697-9_1

[25] DIN German Institute for Standardization. "DIN 1319-3:1996-05, Fundamentals of Metrology - Part 3: Evaluation of Measurements of a Single Measurand, Measurement Uncertainty". Berlin: Beuth Verlag GmbH

## Definitions / Abbreviations

| | |
|---|---|
| $\alpha$ | Crank angle |
| ΔTE | Delta thermal efficiency |
| $\lambda$ | Air–fuel equivalence ratio |
| ATDC | After top dead center |
| BEV | Battery electric vehicle |
| BMEP | Brake mean effective pressure |
| BS | Brake specific |
| BTE | Brake thermal efficiency |
| BtL | Biomass to liquid |
| CA | Crank angle |
| CDC | Conventional diesel combustion |
| CDF | Conventional dual-fuel |
| $CH_4$ | Methane |
| $C_3H_8$ | Propane |
| CI | Compression ignition |
| CNG | Compressed natural gas |
| CO | Carbon monoxide |
| $CO_2$ | Carbon dioxide |
| DF | Dual-fuel |
| DI | Direct injection |
| DOHC | Double overhead camshaft |
| E85 | 85 % ethanol, 15 % gasoline |
| ECU | Electronic control unit |
| EGR | Exhaust gas recirculation |
| EV | Exhaust valve |
| GDBF | Gasoline/diesel blend fuels |
| HCCI | Homogeneous charge compression ignition |
| HCII | Homogeneous charge induced ignition |
| HRF | High reactivity fuel |
| $I$ | Cumulative heat release |
| IMEP | Indicated mean effective pressure |
| ITE | Indicated thermal efficiency |
| IV | Intake valve |
| IVC | Intake valve closing |
| $L_{st}$ | Stoichiometric air requirement |
| LHV | Lower heating value |
| LPG | Liquefied petroleum gas |
| LRF | Low reactivity fuel |
| LTC | Low temperature combustion |
| $m$ | Mass |
| $\dot{m}$ | Mass flow |
| max | Maximum |
| min | Minimum |
| $M$ | Molar mass |
| MON | Motor octane number |
| NO | Nitrogen monoxide |
| NOx | Nitrogen oxides |
| NRSC | Non-road steady cycle |
| $O_2$ | Oxygen |
| OHV | Overhead valves |
| $P_e$ | Brake engine power |
| PCCI | Premixed charge compression ignition |
| PCI | Premixed compression ignition |
| PCO | Premixed charge operation |
| PFO | Premixed fuel operation |
| PM | Particulate mass |
| PN | Particulate number |
| POMDME | Poly oxymethylene dimethyl ethers |
| RCCI | Reactivity controlled compression ignition |
| SE | Second event |
| SR | Substitution rate |
| TDC | Top dead center |
| THC | Total hydrocarbons |
| VVL | Variable valve lift |
| WHSC | World harmonized stationary cycle |
| $x_{Substitution}$ | Substitution rate |

# Appendix

Table 5: Overview over measured and calculated values including accuracies and uncertainties according to DIN 1319-3 [25]

| Value | Measurement Device | Measurement Method | Accuracy | Percentage Uncertainty |
|---|---|---|---|---|
| Speed | Schenck W400 | Pulse Generator | ± 1 $min^{-1}$ | 0.01 |
| Force | HBM U2B | Load Cell | ± 10 N | 0.02 |
| Fuel Mass Flow Diesel | AVL Fuelexact | Coriolis Flow Meter | ± 0.1 % + 0.002 kg/h | 0.06 |
| Fuel Mass Flow Biopropane | E&H Cubemass C300 | Coriolis Flow Meter | ± 0.1 % | 0.10 |
| Air Mass Flow | Sensyflow FMT700-P | Hot Wire Sensor (MAF) | ≤ ± 1 % | 0.02 |
| THC Concentration | Horiba MEXA-7170DEGR | Flame Ionization Detector | ≤ ± 1 % | 0.06 |
| CO Concentration | Horiba MEXA-6000FT | Fourier-Transform Infrared Spectroscopy | ≤ ± 1 % | 0.24 |
| $CO_2$ Concentration | Horiba MEXA-6000FT | Fourier-Transform Infrared Spectroscopy | ≤ ± 1 % | 0.05 |
| $CO_2$ Concentration (Intake) | Horiba MEXA-7170DEGR | Nondispersive Infrared Sensor | ≤ ± 1 % | 0.19 |
| NOx Concentration | Horiba MEXA-6000FT | Fourier-Transform Infrared Spectroscopy | ≤ ± 1 % | 0.12 |
| Soot Concentration | AVL Micro Soot | Photoacoustic | ≤ 0.01 $mg/m^3$ | 0.26 |
| Fuel Temperature | Omega PT100 | Resistance Thermometer | (0.15+0.002*T) °C | 0.01 |
| Cylinder Pressure | Kistler 6056 | Piezoelectric | ≤ ± 0.5 bar | 0.50 |
| Crank Angle | Heidenhain ROD 426 | Photoelectric Incremental Encoder | ± 0.005 ° | 0.001 |
| Brake Power | - | Calculated | - | 0.022 |
| Exhaust Mass Flow | - | Calculated | - | 0.013 |
| Fuel Mass Combined | - | Calculated | - | 0.047 |
| Air–Fuel Equivalence Ratio | - | Calculated | - | 0.049 |
| THC Brake Specific | - | Calculated | - | 0.065 |
| CO Brake Specific | - | Calculated | - | 0.241 |
| NOx Brake Specific | - | Calculated | - | 0.123 |
| Soot Brake Specific | - | Calculated | - | 0.261 |
| EGR-Rate | - | Calculated | - | 0.196 |
| Brake Thermal Efficiency | - | Calculated | - | 0.052 |
| Indicated Thermal Efficiency | - | Calculated | - | 0.502 |